Second Derivatives of Photoplethysmogram for Hyperuricemia Classification using Artificial Neural Network

Hafifah Ab Hamid
Department of Electrical, Electronic & Systems Engineering
Universiti Kebangsaan Malaysia
Bangi, Malaysia
p98362@siswa.ukm.edu.my

Nazrul Anuar Nayan
Department of Electrical, Electronic & Systems Engineering
Universiti Kebangsaan Malaysia
Bangi, Malaysia
nazrul@ukm.edu.my

Mohd Zubir Suboh
Department of Electrical, Electronic & Systems Engineering
Universiti Kebangsaan Malaysia
Bangi, Malaysia
p98999@siswa.ukm.edu.my

Amalia Aminuddin
Department of Physiology
Universiti Kebangsaan Malaysia
Cheras, Kuala Lumpur, Malaysia
amyyra1234@yahoo.com.my

2020 IEEE-EMBS Conference on Biomedical Engineering and Sciences (IECBES) | 978-1-7281-4245-6/21/$31.00 ©2021 IEEE | DOI: 10.1109/IECBES48179.2021.9398786

***Abstract*— Hyperuricemia, a condition in which uric acid level in the blood increases, is associated with cardiovascular disease risk. Elevated uric acid level due to excessive purines deposited at the joint (urate) can cause gout and the formation of urate renal stones. Patients with high serum uric acid (SUA) levels must undergo a blood screening test, which is invasive and costly and requires traveling on the scheduled date. In this paper, the second derivative of photoplethysmogram (SDPPG) is used in analyzing the association between SUA levels and photoplethysmogram (PPG) morphology. A total of 34 features were extracted from the left and right hands of 74 subjects. The features included amplitude-derived (pulse height, amplitude difference, ratio, and jerk) and interval-derived (intervals and relative crest time) of SDPPG features. The features were evaluated using *t*-test statistical analysis for the selection of features, which would be input to machine learning. An artificial neural network and variable number of neurons were used in producing accurate results. The developed model showed sensitivity, specificity, and accuracy of 90.91% in the prediction of high and low SUA levels for both genders. Therefore, the use of PPG and machine learning technique for the noninvasive monitoring of preliminary and regular SUA levels is recommended.**

Keywords — second derivative of photoplethysmogram, artificial neural network, hyperuricemia.

I. INTRODUCTION

Hyperuricemia has been a major health problem worldwide. In addition to contributing to gout and nephrolithiasis or formation of kidney stones, hyperuricemia is associated with numerous comorbidities, such as diabetes, cardiovascular disease, metabolic syndrome, and chronic kidney disease [1-2]. Serum uric acid (SUA) is the final product of the endogenous purine metabolism and exogenous pool (diet) [3]. Purine rich food (>300 mg/100 g) includes anchovy, cutlass fish, and dried yeast [4]. Elevated SUA concentration is caused by low renal excretion rates and SUA overproduction [5]. Hyperuricemia is defined as SUA of >420 µmol/L for males and >360 µmol/L for females [6].

Currently, SUA level is measured invasively through blood tests. Few studies investigated the association of SUA level with brachial–ankle [7-8] and carotid–femoral [9] pulse wave velocities by using photoplethysmogram (PPG). In both cases, two points are needed in finding the association between SUA level and PPG morphology. Hence, a simple yet reliable way for measuring SUA level with an optical method must be established, specifically with the use of PPG as a preliminary diagnostic tool replacing blood test and two-point PPG.

PPG is a promising technique for analyzing many physiological parameters, such as heart compliance, blood viscosity, vessel elasticity, microvascular blood flow, and tissue viability [10]. PPG signals are responsive to changes in blood volume. Therefore, PPG optically detects and records changes in blood volume in the sensor coverage area and generates PPG signal [11]. Given that PPG has been widely used in measuring heart rate and blood pressure [10], it can provide useful information about the cardiovascular system, including arterial pulses.

The recent application of machine learning (ML) technique for SUA classification has been conducted in Korea [12], Japan [13], and Bangladesh [14]. Sociodemographic characteristics, clinical measurements, and dietary information are ML inputs for predicting SUA level. Performance was measured in terms of sensitivity, specificity, and root mean square error. ML is a promising technique for predicting SUA level. However, ML is rarely used in predicting SUA level on the basis of PPG data, which are widely used in various applications in the clinical set up.

The second derivative of PPG (SDPPG) has been widely used as a simple and reliable measure technique for pressure augmentation during clinical investigation [12]. The SDPPG is a double differentiation of the PPG wave, which not only serves as a marker of vascular aging [13] but also is closely associated with cardiovascular risk indicators [14]. Five fiducial points, namely, a, b, c, d, and e peaks, can be extracted from SDPPG. The SDPPG waveform is preferred by researchers analyzing the PPG waveform contour, which is difficult to use, because the SDPPG waveform can be emphasized and easily quantified according to delicate changes in the PPG contour [15]. Furthermore, the morphological features of SDPPG are closely related to vessel condition [16] in which SUA is found.

In this paper, a set of PPG signals from hyperuricemia patients (case) were compared with PPG signals obtained from healthy subjects (controls). The features of SDPPG, or

acceleration PPG, were analyzed as high SUA level parameters, which included SDPPG pulse height, amplitude difference, ratios, intervals, relative crest time (RCT), and jerks. Fig. 1 shows the block diagram of the proposed method for SUA level PPG signal classification.

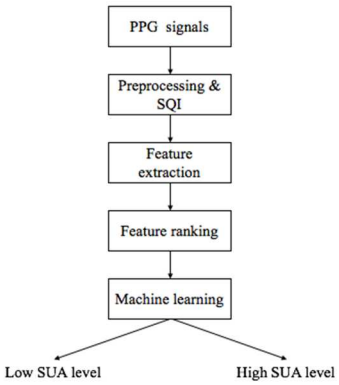

Fig. 1. Block diagram of SUA level classification methodology.

II. METHODOLOGY

A. Subjets and Protocol

The Research and Ethics Committee of the Hospital Universiti Kebangsaan Malaysia approved the study, which received a registration number of UKM.PPI.800-1/3/21. A total of 74 nonsmoking control and case subjects participated in the study. Each participant provided oral and written informed consent.

The recruited subjects were enrolled on the basis of their histories and health status. A total of 37 controls (20 males and 17 females) had normal SUA levels, and 37 case subjects (22 males and 15 females) were recruited from Pusat Perubatan UKM, Klinik Primer UKM and Pusat Kesihatan Universiti, UKM. The controls and case subjects were 19 to 80 years old.

PPG signals were detected from the fingertips for both hands of the subjects in supine position. The signals were recorded for 10 min with pulse oximeter sensors (CMS 50D+) at a sampling frequency of 100 Hz. Blood test for gold standard SUA level measurement was taken for each control and case subject. MATLAB software was used for signal processing.

B. Preprocessing and SQI

The acquired PPG signals were filtered using a 4th order Bessel bandpass filter (0.8–8 Hz) for the removal of the respiratory rhythm effect and high-frequency disturbance. Anything below 0.5 Hz was attributed to baseline wandering, anything above 8 Hz was considered high-frequency noise. Auto-offsetting was used in overcoming amplitude offset after the cleaning process. Any y-axis value below zero was brought back to a positive value by offsetting the signal with the difference between zero-amplitude and largest negative value detected. Then, the cleaned signal was processed through signal quality indexing (SQI).

High-quality PPG signals refer to stable signals within a period of time that have no external interference factors that may change subsequent processing results. SQI is a method for evaluating signal quality. The three conditions that must be fulfilled for the PPG signal were as follows: (1) PPG signal extrapolated from 10 s sample must be between 40 and 180 beats per minute, (2) PPG pulse-peaks gap must not exceed 3 s in order that not more than one beat is missed, and (3) the ratio of the maximum beat to beat interval to the minimum beat to beat interval within a sample should be less than 2.2 [17]. Then, only high-quality PPG signals were applied to two times of differentiation for the generation of an SDPPG wave.

C. Feature Extraction

The four fiducial points detected from PPG signals are pulse onset, systolic, dicrotic notch, and diastolic peak, as shown in Fig. 2. (a). The determination of pulse onset in which the moving average of the second derivative is larger than the adaptive threshold. The systolic peak is the maximum waveform after foot and is relative to a window of radius 1/8 s around the detected peak. The dicrotic notch is the minimum value of the subtracted signal and the straight line going from systole to diastole. The diastolic peak is the minimum of second derivative following the dicrotic notch and is relative to a window of radius systolic to systolic peak (median heartbeat interval obtained using foot indices) divided by 5 s around itself.

SDPPG peaks were determined according to each detected systolic peak adapting to the algorithm proposed in [18] with some modification. The maximum and minimum peaks of first derivative of PPG (FDPPG) were determined first and used as references for the detection of all SDPPG peaks. The maximum peak obtained by finding all positive peaks and the first peak that occurred before systolic peak and after onset was labeled as the "maximum peak." This approach is different from that used in [18], wherein threshold was set for the identification of the most significant peak. The low amplitude of the maximum peak caused false peak detection. For the minimum peak, all the negative peaks and negative peaks that occurred after the maximum peak of FDPPG and before half of the duration of the current cycle were labeled as "minimum peaks." Fig. 2. (b) shows minimum and maximum peak determination.

Five peaks from the SDPPG waveform were extracted, namely, a, b, c, d, and e. Fig. 2. (c) shows the five detected peaks. The process of inflection point detection is shown in Fig. 2. The definition of five peak detection are as following:

"a" peak: the "a" peak can be easily located using the maximum peak location in SDPPG, wherein the first positive peak before the maximum peak of FDPPG can be considered an "a" peak.

"b" peak: all negative peaks and the first negative peak that occurred after the zero-crossing of the "a" peak.

"c" and "d" peaks: in the presence of another wave or curve (positive and negative peaks) between "b" and "e" peaks, the first negative peak before the "e" peak was the "d" peak, and the first positive peak before the "d" peak was the "c" peak. Otherwise, the "c", "d", and "e" peaks were considered to have merged into a single peak ("e" peak).

"e" peak: Through observation, the maximum range of the "e" peak was found before dicrotic notch detected in the raw PPG signal.

The developed feature extraction algorithm managed to detect the "a", "b", "c", "d", and "e" peaks correctly from SDPPG waveform, as shown in Fig. 2. The "a" peak is the first positive peak and thus more easily detected than the maximum peak with the threshold in [18]. As suggested in [18], the "e" lies within the minimum peak and local extreme peak in

FDPPG. Thus, finding local extreme peak is a complicated process.

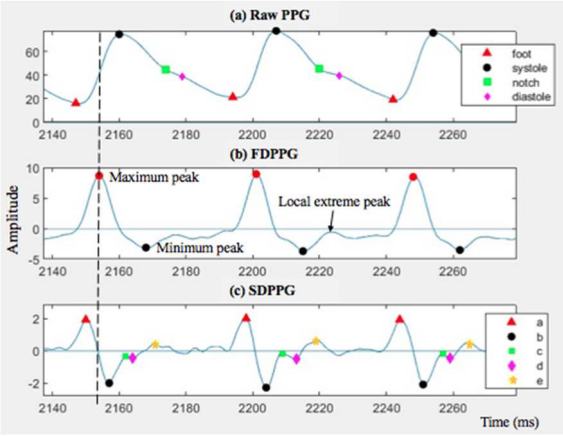

Fig. 2. Description of (a) raw PPG waveform, (b) FDPPG and (c) SDPPG waveform.

In this study, fifty-one features were identified from the SDPPG on the basis of five fiducial peaks, as shown in Table I. However, the "c", "d", and "e" peaks were merged into a single peak (peak "e") in some subjects. According to [19], the probable cause was the fast heart rate. Hence, by removing all features that involve "c" and "d" peaks, only 17 features were used in this study for each hand.

TABLE I. AVAILABLE FEATURES FROM SDPPG

No.	Type of features	Total	Feature label	Description
1	Peak amplitude	5	a, b, c, d, e	Amplitude from 0 value of arbitrary unit to a peak
2	Peak ratio	10	Rab, Rac, Rad, Rae, Rbc, Rbd, Rbe, Rcd, Rce, Rde	Ratio of 2 peak amplitude
3	Amplitude difference	10	Aab, Aac, Aad, Aae, Abc, Abd, Abe, Acd, Ace, Ade	Difference between 2 peak amplitude
4	Peak interval	10	Tab, Tac, Tad, Tae, Tbc, Tbd, Tbe, Tcd, Tce, Tde	Interval between 2 peak in time domain
5	Jerk	10	Jab, Jac, Jad, Jae, Jbc, Jbd, Jbe, Jcd, Jce, Jde	Absolute height of 2 respective waves with the corresponding time interval
6	RCT	4	RCTab, RCTac, RCTad, RCTae	Ratio of extracted interval compared with the pulse width
7	Aging index & vascular age	2	AGI, VA	AGI = (b-c-c-e)/a VA = 45.5(b-c-d-e) + 65.9

D. Feature Ranking

A total of 34 features were extracted from the SDPPG signals from left and right hands. The extracted features of the SDPPG, namely, pulse height, amplitude difference, ratio, interval, RCT, and jerk, were analyzed statistically with SPSS software. The descriptive statistics of the features were expressed as mean ± SD. The features were ranked according to the least *p*-value with independent sample *t*-test for low SUA and high SUA groups. Features with *p*-values lower than 0.05 (confidence interval of 95%) were considered statistically significant. High-ranked features were used as inputs for the ML algorithm.

E. Machine Learning

Artificial neural network (ANN) is a promising ML technique for classification. Recent research compared few types of ML in terms of performance in predicting CVD with electrocardiogram waveform and showed that an ANN have a higher performance than other ML techniques [20]. ANNs had been used in automatically detecting premature ventricular contractions [21]. In the present study, the number of hidden neurons was set from 1 to 40 because an enormous number of inputs were obtained from the PhysioNet MIMIC II database for ANN ML technique. A study on Brazil population compared ANN and logistic regression as predictive tools and showed that ANN showed the highest accuracy in predicting mortality in intensive care units [22]. The advantage of ANNs as predictive tools is their incorporate nonlinear effects. In this study, an ANN was selected as an ML method. As shown in Fig. 3, a three-layer feed-forward network was used along with the "trainlm" algorithm, "logsig" transfer function at hidden layers, and "purelin" transfer function at the output layer. The input is the number of features selected, whereas the output was set at "0" for the control group and "1" for the case group. The numbers of hidden neurons at first and second layer varied from 1 to 20 for the establishment of the best classifier model on the basis of specificity, sensitivity, and accuracy.

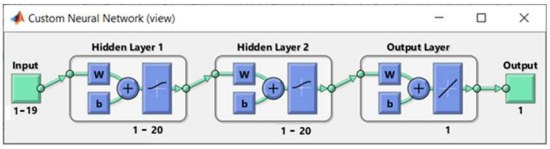

Fig. 3. ANN structure

Specificity, sensitivity, and accuracy were given by

$$Specificity = \frac{TN}{TN + FP} \times 100\% \quad (1)$$

$$Sensitivity = \frac{TP}{TP + FN} \times 100\% \quad (2)$$

$$Accuracy = \frac{TP+TN}{TP + FP+TN+FN} \times 100\% \quad (3)$$

where TN is true negative, TP is true positive, FP is false positive, and FN is false negative.

III. RESULT AND DISCUSSION

The statistic value for each feature in both groups was ranked according to the smallest *p*-value and presented as mean ± SD, as shown in Table II. The first letter in the feature label refers to the right- or left-hand feature. The two features are statistically significant, namely, the time interval between the "a" and "b" peaks of the right hand (RTab) and pulse jerk between the "b" and "e" peaks between the left hand. However, more data is required to increase classification accuracy. Another 17 features ($p < 0.5$) were selected as inputs for the ANN classifier. All the 19 features in Table I are important in differentiating both groups, except AGI and VA given that the "c" and "d" peaks are not available for all SDPPG signals.

A total of 74 subjects with 148 PPG recordings (left and right hands) were used in training and testing the network. Data was randomly distributed in 70:30 ratio as train and test data. ANN was trained with varying number of hidden neurons and features selected through feature ranking. Specificity, sensitivity and accuracy were determined and recorded as demonstrated in Fig. 4.

TABLE II. THE MEAN ± SD OF FEATURES EXTRACTED FROM CONTROL AND CASE GROUP ARRANGED FROM SMALLEST TO BIGGEST P-VALUES

No.	Feature	Control		Case		*p*-value
		Mean	SD	Mean	SD	
1	RTab	0.0673	0.0056	0.0645	0.0051	0.03*
2	LJbe	13.0785	4.4838	15.4851	5.4300	0.04*
3	LJae	4.7056	1.4514	5.3647	1.7018	0.08*
4	LJab	43.7702	16.3237	49.6349	16.3960	0.13*
5	RRab	-1.0242	0.1867	-0.9646	0.1778	0.16*
6	LTab	0.0682	0.0071	0.0662	0.0056	0.18*
7	LRab	-1.0537	0.2007	-0.9931	0.1890	0.19*
8	Lb	-1.5462	0.6105	-1.7302	0.5837	0.19*
9	LRbe	-3.4895	0.9796	-3.7842	0.9614	0.20*
10	LTae	0.2295	0.1254	0.2030	0.0167	0.21*
11	RRCTab	0.1256	0.0169	0.1199	0.0239	0.24*
12	RRCTae	0.3849	0.0391	0.3715	0.0580	0.25*
13	RRae	3.6399	1.0450	3.3933	0.8717	0.27*
14	LTbe	0.1601	0.1275	0.1369	0.0145	0.27*
15	RAae	1.0560	0.2010	1.0083	0.1756	0.28*
16	La	1.5052	0.4008	1.5981	0.3781	0.31*
17	RJab	48.1823	14.3779	51.3009	16.8598	0.39*
18	RJbe	15.2397	4.7583	16.2120	6.2732	0.46*
19	LRCTae	0.3860	0.0445	0.3787	0.0443	0.48*
20	Re	0.4842	0.1522	0.5056	0.1478	0.54
21	Ra	1.6310	0.3380	1.5815	0.3653	0.55
22	RAab	3.0844	0.6000	3.0078	0.5823	0.58
23	LRae	3.5634	0.8677	3.6771	0.9672	0.60
24	LRCTab	0.1256	0.0272	0.1229	0.0185	0.62
25	RAbe	2.0310	0.4159	1.9840	0.4252	0.63
26	LAbe	1.9662	0.4189	1.9272	0.3950	0.68
27	RJae	5.3927	1.5742	5.2602	1.6289	0.72
28	RTae	0.2050	0.0134	0.2041	0.0174	0.79
29	LAae	1.0332	0.2169	1.0213	0.1824	0.80
30	RRbe	-3.6372	1.2179	-3.5765	0.9475	0.81
31	LAab	3.0027	0.6158	2.9776	0.5222	0.85
32	Rb	-1.7240	0.5452	-1.7410	0.6018	0.90
33	RTbe	0.1377	0.0147	0.1373	0.0154	0.91
34	Le	0.4644	0.2013	0.4657	0.1533	0.97

* Indicated significant *p*-value ($p < 0.5$)

As shown in Fig. 4, some of the trained networks have 100% specificity (when 18 features were used) and 100% sensitivity (when 12,13,17, or 19 features were used). This result shows that the effectiveness of using SDPPG features in differentiating control and case groups. In general, accuracy increases with the number of features (up to 15 features). The best network has an accuracy of 90.91%, with equal specificity and sensitivity, (two misclassified data from a total of 22 test data). This network was trained using 15 features; five at first hidden layers, and seven neurons at second hidden layers. Fig. 5 shows the validation performance established for the training, validation, and test steps. The best performance was observed in the epoch with the lowest validation error. According to Fig. 5, the best validation performance was observed at epoch 6, which has the least mean square error of 0.21597.

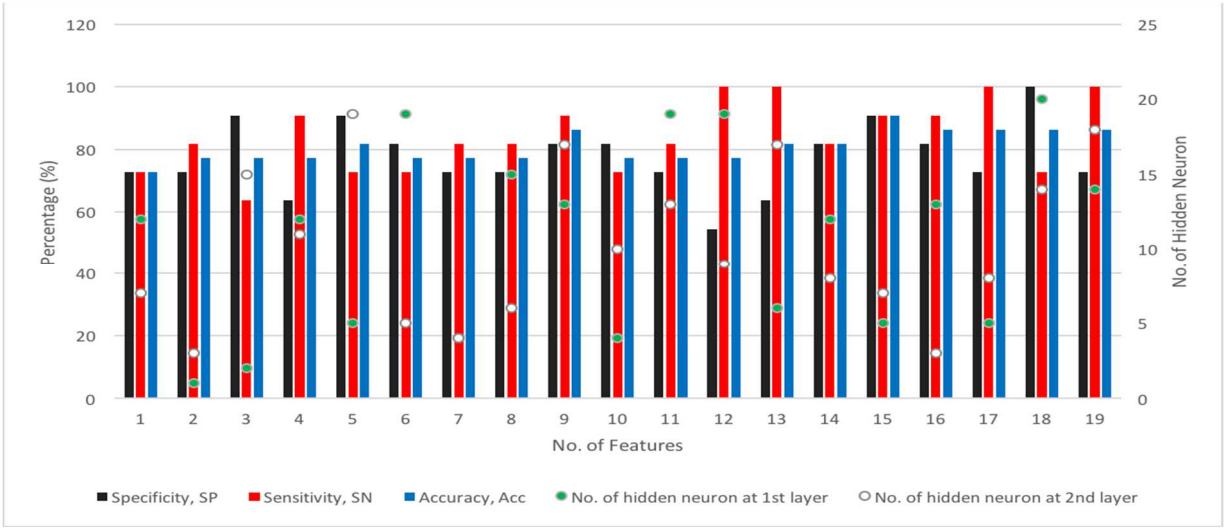

Fig. 4. ANN performance with different number of features and hidden neurons.

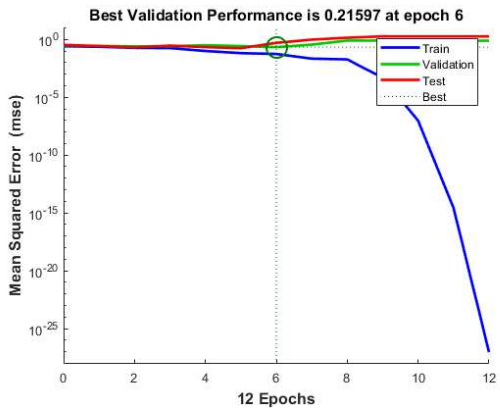

Fig. 5. Best validation performance in the ANN model.

IV. CONCLUSION

This study demonstrated that PPG can be used as a preliminary SUA level diagnosing tool and complements the currently existing invasive "gold standard" SUA level measurement. The algorithm proposed in detecting "a", "b", "c", "d", and "e" peaks from the SDPPG waveform showed promising results. As highlights, the "a" and "e" peaks were more easily defined than those in a previously researched algorithm. The classification model, ANN acquired inputs from a combination of SDPPG features from case and control subjects. It showed sensitivity, specificity, and accuracy of 90.91% in distinguishing the features from the case and control subjects by using 15 SDPPG features.

ACKNOWLEDGMENT

The authors would like to thank the Ministry of Education, Malaysia and Universiti Kebangsaan Malaysia for supporting this research through research grant GUP-2019-020.

REFERENCES

[1] R. Liu, C. Han, D. Wu, X. Xia, J. Gu, H. Guan, Z. Shan, and W. Teng, "Prevalence of hyperuricemia and gout in mainland China from 2000 to 2014: a systematic review and meta-analysis," BioMed research international, 2015.

[2] M. Sellmayr, M. R. H. Petzsche, Q. Ma, N. Kruger, H. Liapis, A. Brink, B. Lenz, M. L. Angelotti, V. Gnemmi, C. Kuppe, and H. Kim, "Only Hyperuricemia with Crystalluria, but not Asymptomatic Hyperuricemia, Drives Progression of Chronic Kidney Disease," Journal of the American Society of Nephrology, 2020.

[3] J. Maiuolo, F. Oppedisano, S. Gratteri, C. Muscoli, and V. Mollace, "Regulation of uric acid metabolism and excretion," International journal of cardiology, vol. 213, pp.8-14, 2016.

[4] K. Kaneko, F. Takayanagi, T. Fukuuchi, N. Yamaoka, M. Yasuda, K. I. Mawatari, and S. Fujimori, "Determination of total purine and purine base content of 80 food products to aid nutritional therapy for gout and hyperuricemia," Nucleosides, Nucleotides & Nucleic Acids, pp.1-9, 2020.

[5] B. Rivera-Paredez, L. Macías-Kauffer, J. C. Fernandez-Lopez, M. Villalobos-Comparán, M. M. Martinez-Aguilar, A. de la Cruz-Montoya, E. G. Ramírez-Salazar, H. Villamil-Ramírez, M. Quiterio, P. Ramírez-Palacios, and S. Romero-Hidalgo, "Influence of Genetic and Non-Genetic Risk Factors for Serum Uric Acid Levels and Hyperuricemia in Mexicans," Nutrients, vol. 11, no. 6, p.1336, 2019.

[6] X. Zheng, Q. Wei, J. Long, L. Gong, H. Chen, R. Luo, W. Ren, and Y. Wang, "Gender-specific association of serum uric acid levels and cardio-ankle vascular index in Chinese adults," Lipids in health and disease, vol. 17, no. 1, pp.1-6, 2018.

[7] F. Luo, and C. Zhuo, "Association between uric acid and brachial-ankle pulse wave velocity: secondary analysis of data from a cross-sectional study," Scientific Reports, vol. 10, no. 1, pp.1-8, 2020.

[8] S. Nagano, M. Takahashi, N. Miyai, M. Oka, M. Utsumi, M. Shiba, K. Mure, T. Takeshita, and M. Arita, "Association of serum uric acid with subsequent arterial stiffness and renal function in normotensive subjects," Hypertension Research, vol. 40, no. 6, pp.620-624, 2017.

[9] M. Canepa, F. Viazzi, J. B. Strait, P. Ameri, R. Pontremoli, C. Brunelli, S. Studenski, L. Ferrucci, E. G. Lakatta, and M. AlGhatrif, "Longitudinal association between serum uric acid and arterial stiffness: results from the Baltimore longitudinal study of aging," Hypertension, vol. 69, no. 2, pp.228-235, 2017.

[10] J. Allen, "Photoplethysmography and its application in clinical physiological measurement," Physiol Meas., vol. 28, pp.1–39. 2007.

[11] M. Elgendi, R. Fletcher, Y. Liang, N. Howard, N. H. Lovell, D. Abbott, K. Lim, and R. Ward, "The use of photoplethysmography for assessing hypertension," NPJ digital medicine, vol. 2, no. 1, pp.1-11, 2019.

[12] J. Hashimoto, K. Chonan, Y. Aoki, T. Nishimura, T. Ohkubo, A. Hozawa, M. Suzuki, M. Matsubara, M. Michimata, T. Araki, and Y. Imai, "Pulse wave velocity and the second derivative of the finger photoplethysmogram in treated hypertensive patients: their relationship and associating factors," Journal of hypertension, vol. 20, no. 12, pp.2415-2422, 2002.

[13] M. Elgendi, "On the analysis of fingertip photoplethysmogram signals," Curr. Cardiol. Rev., vol. 8, no. 1, pp.14–25, 2012.

[14] J. A. Laukkanen, R. and Rauramaa, "Systolic blood pressure during exercise testing and the risk of sudden cardiac death," Int. J. Cardiol., vol.. 168, no. 3, pp.3046–3047, 2013.

[15] M. Elgendi, R. R. Fletcher, I. Norton, M. Brearley, D. Abbott, N. H. Lovell, and D. Schuurmans, "Frequency analysis of photoplethysmogram and its derivatives," Computer methods and programs in biomedicine, vol. 122, no. 3, pp.503-512, 2015.

[16] M. Liu, L. M. Po, and H. Fu, "Cuffless blood pressure estimation based on photoplethysmography signal and its second derivative," International Journal of Computer Theory and Engineering, vol. 9, no. 3, p.202, 2017.

[17] C. Orphanidou, T. Bonnici, P. Charlton, D. Clifton, D. Vallance, and L. Tarassenko, "Signal-quality indices for the electrocardiogram and photoplethysmogram: Derivation and applications to wireless monitoring," IEEE journal of biomedical and health informatics, vol. 19, no. 3, pp.832-838, 2014.

[18] A. Chakraborty, D. Sadhukhan, and M. Mitra, "An Automated Algorithm to Extract Time Plane Features From the PPG Signal and its Derivatives for Personal Health Monitoring Application," IETE Journal of Research, pp.1-13, 2019.

[19] M. Elgendi, "Detection of c, d, and e waves in the acceleration photoplethysmogram," Computer methods and programs in biomedicine, vol. 117, no. 2, pp.125-136, 2014.

[20] N. A. Nayan, H. A. Hamid, M. Z. Suboh, N. Abdullah, R. Jaafar, N. A. Yusof, M. A. Hamid, N. F. Zubiri, A. S. Arifin, S. M. A. Daud, M. A. Kamaruddin, "Cardiovascular disease prediction from electrocardiogram by using machine learning", International Journal of Online and Biomedical Engineering, vol. 17, no. 7, pp.34-48, 2020.

[21] A. Solosenko, A. Petrenas, and V. Marozas, "Photoplethysmography-based method for automatic detection of premature ventricular contractions", IEEE Transactions on Biomedical Circuits and Systems, vol. 9, no. 5, pp.662-669, 2015.

[22] K. K. de Souza, and J. L. B. Marques, "Use of photoplethysmography to predict mortality in intensive care units", Vascular Health and Risk Management, vol. 14, pp.311-320, 2018.